Research Article

Visible Light Induced Photocatalytic Degradation of Methyl Red with Codoped Titania

Susmitha Thota,[1] Siva Rao Tirukkovalluri,[1] and Sreedhar Bojja[2]

[1] Department of Inorganic & Analytical Chemistry, School of Chemistry, Andhra University, Visakhapatnam 500 003, India
[2] Department of Chemistry, CSIR-Indian Institute of Chemical Technology, Hyderabad 500 007, India

Correspondence should be addressed to Siva Rao Tirukkovalluri; sivaraotvalluri.16@gmail.com

Photocatalysis using semiconductor oxides was being investigated extensively for the degradation of dyes in effluent water. This paper reports our findings on visible light induced photocatalytic degradation of azo dye, methyl red mediated nitrogen and manganese codoped nano-titanium dioxide (N/Mn-TiO$_2$). The codoped samples with varying weight percentages were synthesized by sol-gel method and characterized by various analytical techniques. The X-ray diffraction data showed that the synthesized samples were in anatase phase with 2θ at 25.3°. UV-visible diffuse reflectance spectral analysis revealed that the presence of dopants in TiO$_2$ caused a significant absorption shift towards visible region and their presence was confirmed by X-ray photoelectron spectral data. The release of hydroxyl radical (major active species in photocatalytic degradation) by the photocatalyst in aqueous solution under visible light irradiation was quantitatively investigated by the photoluminiscent technique (PL). The effect of various experimental parameters like dopant concentration, pH, catalyst dosage, and initial dye concentrations was investigated and optimum conditions were established. The extent of mineralization of methyl red was studied by chemical oxygen demand (COD) assays and the results showed complete mineralization of the dye.

1. Introduction

Dyes are the resistant compounds that are found in industrial waste water causing adverse environmental problems. Most of the dyes used in the pigmentation of textiles, leather, paper, ceramics, and food-processing are derived from azo dyes. Approximately 15% of these are lost with waste water during synthesis and processing [1]. This represents a great hazard to human and environmental health due to the toxicity of azo dyes [2]. The treatment of such pollutants can be achieved by heterogeneous photocatalysis due to its efficiency and low cost as well as to the fact that it allows complete degradation of pollutants to carbon dioxide and inorganic acids [3].

TiO$_2$ has attracted a great deal of study for its high photocatalytic activity. But the fatal drawbacks of TiO$_2$ are its wide band gap and high rate of electron-hole (e$^-$/h$^+$) recombination [4]. A number of studies have been reported on the modification of TiO$_2$ in order to extend the absorption of light to the visible region. These include dye sensitization, semiconductor coupling, impurity doping, use of

coordination metal complexes, and metal deposition [5]. Among all these methods, codoping TiO$_2$ with a metal and nonmetal is found to be most suitable. According to literature survey, the nonmetal dopant reduces the band gap making it active in visible region and metal dopant facilitates the charge separation of e$^-$/h$^+$ and thus decreases their rate of recombination [6]. Besides, considering the significance of visible light responsive photocatalyst, it is very interesting to search for new photocatalyst with appropriate crystal phase, particle size, and other surface properties to improve the photocatalytic activity. Hence in our research work we have selected nitrogen (N) and manganese (Mn) as nonmetal and metal dopants to be codoped in TiO$_2$ and study its photocatalytic activity by degrading a model azo dye pollutant, methyl red.

Various methods available for the synthesis of TiO$_2$ photocatalyst include precipitation [7], hydrothermal, solvothermal [8], chemical vapour deposition [9], and electrospinning [10]. Among several methods available for synthesis of nanopowders, sol-gel method is advantageous because

powders of homogenous concentrations and high purity can be synthesized at very low temperatures and high purity can be synthesized at low temperature under stoichiometry control [11]. Hence, sol-gel method has been followed for the synthesis of nitrogen and manganese codoped TiO_2 (N/Mn-TiO_2) photocatalysts.

1.1. Synthesis of Photocatalysts. A series of TiO_2 samples were prepared by codoping with nitrogen and manganese in the range of 0.25–1.00 wt% along with undoped TiO_2 by sol-gel method. For preparation of undoped TiO_2 ethanol is taken as solvent and water was added to titanium tetrabutoxide (titanium precursor) for hydrolysis and condensation reactions to take place in presence of nitric acid. In case of codoped catalyst preparation, calculated quantities of manganese nitrate and urea, precursors of Mn and N, were first dissolved in ethanol along with water and the resultant solution was added drop by drop to the ethanol solution of $Ti(OBu)_4$ under vigorous stirring. After complete addition, the colloidal suspension was allowed to stir for 90 min and aged for 48 hrs. Thus obtained gel was dried in an oven at 70°C. Later, it was well ground and calcined at 400°C for about 5 hrs in muffle furnace at the rate of 2°/min and then cooled in a desiccator and ground to form homogenous powder.

1.2. Characterisation of Photocatalysts. XRD spectra were recorded for 2θ from 20° to 80° with model Ultima IV, RIGAKU diffractometer using monochromatized CuKα radiation (λ = 1.541 Å) with a Germanium solid state detector. The size of the nanoparticles was recorded with a TECNAI FE12 TEM (Eindhonen, The Netherlands) instrument operating at 120 kV. XPS studies were done using PHI quantum ESCA microprobe system model, using AlKα radiation of 250 W X-ray tube as a radiation source with energy of 1486.6 eV, 16 mA × 12.5 kV under working pressure lower than 1×10^{-8} Nm^{-2}. The fitting of the XPS curves was analyzed with multipack 6.0A software. UV-visible absorption spectra of the samples were obtained by using Shimadzu 3600, UV-visible NIR spectrophotometer using $BaSO_4$ as reference scatter. Photoluminescent spectral analysis was done using Horiba Jobin Fluoro Max-4 instrument with a PMT voltage of 150 V and slit set both at 2.5 nm.

1.3. Photocatalytic Activity of Catalyst. Dye solution with catalyst was stirred in dark for 20 min to establish adsorption-desorption equilibrium on the catalyst surface. The reaction mixture was exposed to visible light source of 400 W high pressure mercury vapour lamp (Osram, India) by placing it 20 cm away from light source. At certain regular time intervals, aliquots of samples were collected through 0.45 μm Millipore syringe filter. The filtrate was subjected to COD analysis for mineralization studies at regular time intervals by using acidic dichromate method with a Bioblock COD analyzer. Also, the filtrate was analyzed on spectrophotometer at a wavelength of 525 nm for degradation studies of methyl red and at wavelength of 484 nm for degradation studies of orange II. To have a comprehensive comparison, the reaction environment is maintained the same for all the activity tests. The percentage degradation of dye was calculated from the following equation:

$$\% \text{ of Degradation} = \frac{A_o - A_t}{A_o} \times 100, \tag{1}$$

where A_o is initial absorbance of dye solution before degradation and A_t is absorbance of dye solution at time t.

2. Results and Discussions

2.1. X-Ray Diffraction and Transmission Electron Microscopic Analysis (XRD and TEM). The functionality of TiO_2 for different applications depends on its crystal phase. For photocatalytic applications anatase phase is preferred. The XRD patterns of all the samples exhibited typical peaks at 2θ = 25.3°, 37.7°, 47.9°, and 54.1°, which can be indexed to the (101), (004), (200), and (211) crystal facets of anatase TiO_2 (JCPDS File number: 21-1272). From XRD patterns it is evident that calcinations at 400°C would result in anatase crystal phase transition.

TEM image of 0.75 wt.% N and 0.25 wt.% Mn-TiO_2 (NMN-4) was represented in Figure 1 and average particle size was found to be 9 nm. It is in complete agreement with the results of crystallite size calculated by using the Scherer equation and the full width at half maximum of the (101) peak in the XRD patterns of the material. The particle size of the catalyst plays very important role in its photocatalytic activity. Decrease in particle size results in large surface area which is favorable for high photocatalytic activity.

Based on XRD data and trail photocatalytic activity studies, further characterization has been made for NMN-4 which showed best photocatalytic activity.

2.2. Ultraviolet-Visible Diffuse Reflectance Spectroscopic Studies. The UV-DRS spectral data was shown in Figure 2. It was observed that the synthesized codoped samples had a profound effect on its optical response in the visible wavelength range. Band gap for all the synthesized samples were calculated by using the formula E_g = $(1240/\lambda)$, where E_g is band gap and λ is wavelength [12]. The band gap of synthesized undoped TiO_2 was found to be 3.18 eV which is comparable with the literature value [13]. The codoped samples showed band gap ranging from 2.87 to 3.10 eV. The band gap of NMN-4 was found to be 2.87 eV which has been reduced by 0.31 eV when compared with that of undoped sample. The narrowing of band gap is maybe due to formation of midgap band above valence band by N 2p states. The electrons are transferred from midgap band to conduction band. Thus by narrowing the band gap, the absorbance has shifted from ultraviolet to visible region. Red shift indicates more photogenerated e$^-$/h$^+$ pairs that could be excited by photons with less energy, leading to better photocatalytic degradation efficiency in visible region. Thus, the results demonstrated that all the synthesized codoped samples had reduced band gap and are active in visible region.
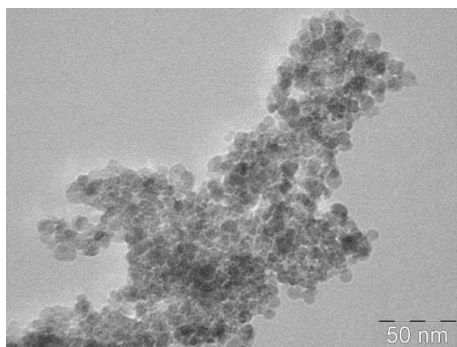
FIGURE 1: TEM image of NMN-4 illustrates the formation of nanoparticles with average particle size of 9 nm.

(a) 0.25 wt.% N and 1.00 wt.% Mn-TiO$_2$
(b) 0.25 wt.% N and 0.75 wt.% Mn-TiO$_2$
(c) 0.50 wt.% N and 0.50 wt.% Mn-TiO$_2$
(d) 0.75 wt.% N and 0.25 wt.% Mn-TiO$_2$
(e) 1.00 wt.% N and 0.25 wt.% Mn-TiO$_2$
(f) 1.00 wt.% N and 0.50 wt.% Mn-TiO$_2$
(g) 0.50 wt.% N and 1.00 wt.% Mn-TiO$_2$
(h) Undoped TiO$_2$

FIGURE 2: UV-visible spectrum of all the synthesized nanocatalysts exhibiting red shift.

2.3. X-Ray Photoelectron Spectroscopic (XPS) Analysis.

XPS measurements of NMN-4 were carried out to confirm the presence of N and Mn and investigate their chemical state. High resolution XPS spectra of NMN-4 with elemental analysis of Ti, O, N, and Mn were represented in Figure 3. In codoped sample, doublet peaks of Mn $2p_{3/2}$ and Mn $2p_{1/2}$ were observed with binding energies of 641.9 and 653.9 eV, respectively. The major peak located at 641.9 eV is attributed to Mn^{3+} with peak area of 75% and the minor peak with higher binding energy of 653.9 eV can be assigned to a higher oxidation state Mn^{4+} [14]. Based on the above XPS data, a reasonable assignment is that Mn exists in both Mn^{4+} and Mn^{3+} states substituting some of the Ti^{4+} in anatase TiO$_2$ lattice giving rise to new electronic interactions. As Mn^{4+}/Mn^{3+} can accept electrons and act as electron trap centre, its doping reduces the rate of e$^-$/h$^+$ recombination. Coming to the N, the binding energy peaks occurred at 399.6 eV. This can be typically assigned as interstitial nitrogen dopant [15]. The XPS spectra of undoped TiO$_2$ show spin-orbit doublet peaks of Ti $2p_{3/2}$ and $2p_{1/2}$ located at 459.0 and 464.7 eV which has peak separation of 5.7 eV indicating the presence of Ti^{4+} in the synthesized nanopowders [16]. The binding energy of Ti $2p_{3/2}$ of codoped sample shifted to a more positive value by 0.7 eV when compared to that of undoped TiO$_2$ that has binding energy of 458.3 eV. Thus the presence of dopants has certain influence on Ti^{4+} pulling the electrons in Ti–O–Ti bond, a bit away from Ti atom, thus causing a little rise in Ti $2p_{3/2}$ binding energy. Thus XPS data has confirmed that there is a substitutional doping of Mn and interstitial doping of N in TiO$_2$ network.

2.4. Photoluminescent Spectral Studies.

Hydroxyl radical is deemed to be one of the crucial reactive species during photocatalytic reaction and is responsible for oxidative decomposition of pollutants. Photoluminescence technique is one of the methods available to investigate the production of $^•$OH. Coumarin is used as a fluorescent probe, which on reaction with $^•$OH results in the formation of 7-hydroxy coumarin [17]. In this technique, 1.0 g/L of catalyst is dispersed in 10 mg/L of coumarin solution in acidic conditions and exposed to visible light radiation. For every 30 min the reaction solutio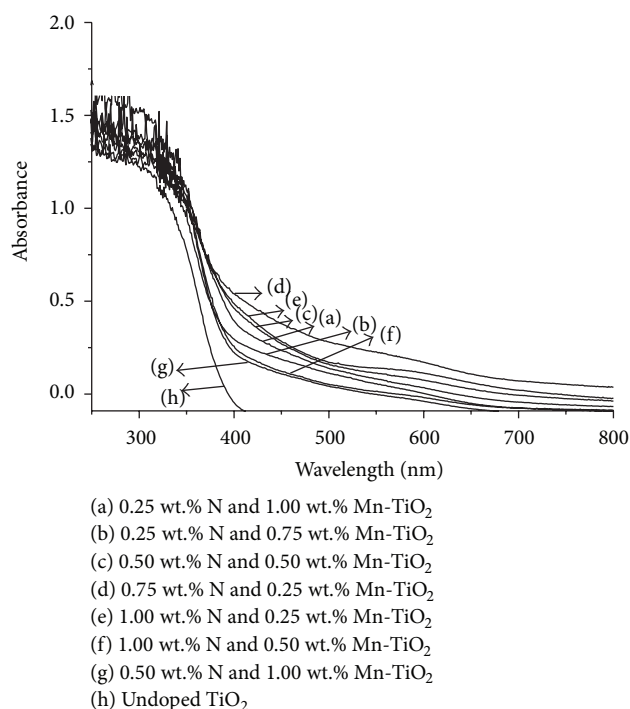n was filtered and photoluminescent intensity was measured from 350 to 600 nm. Figure 4 represents the photoluminescent spectra of the generated 7-hydroxy coumarin with maximum absorption at 450 nm. A linear increase in photoluminescent intensity was observed with increasing irradiation time. However, no maximum absorption is observed for the sample in absence of irradiation (0 min). It could be inferred that the produced $^•$OH at the catalyst surface was proportional to the irradiation time. The results further confirmed that the synthesized sample NMN-4 showed enhanced rate of formation of $^•$OH.

2.5. Photocatalytic Degradation of Methyl Red and Optimization of Parameters.

Photocatalytic degradation of methyl red was performed by following the procedure given in Section 1.3. A blank test with no photocatalyst is also employed. There is no significant change in the concentration of dye. The high photocatalytic performance is dependent on the comprehensively competing effects of the dopant concentration, pH, initial concentration of pollutant, and catalyst dosage. For practical application in industries, degradation of dyes must be cost effective. Hence, these parameters have to be optimized.

2.5.1. Effect of Dopant Concentration.

Photocatalytic degradation studies of different synthesized catalysts with various dopant concentrations on methyl red are presented in Figure 5(a). All the codoped samples showed higher photocatalytic activity than that of Commercial Titania, Degussa P25, under visible light irradiation. So, it is evident that codoping has improved the photocatalytic performance of
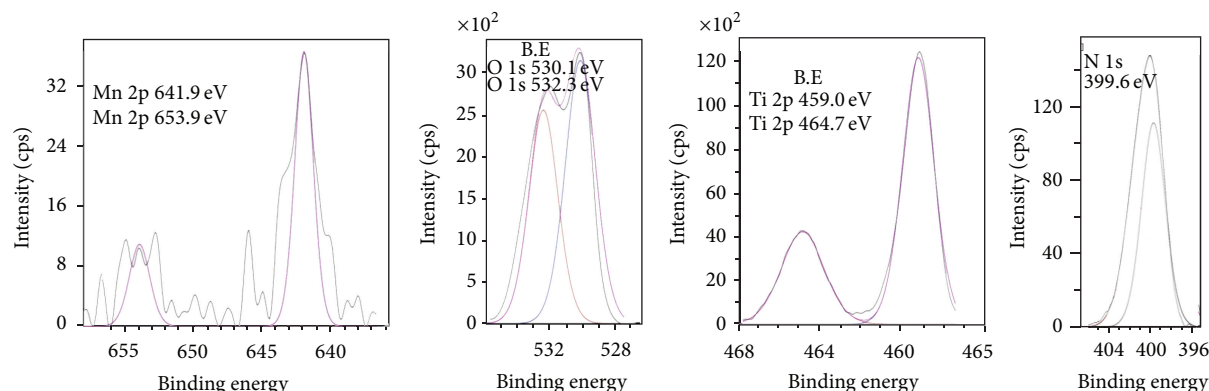
FIGURE 3: High resolution XPS of the 0.75 wt.% N and 0.25 wt.% Mn-TiO$_2$(NMN-4).
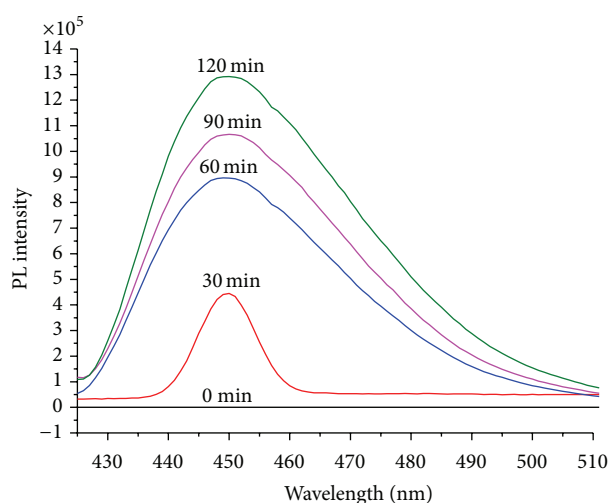

FIGURE 4: PL spectra of NMN-4 indicating the release of OH radicals when exposed to visible light. The rate of release is very high in first 60 min and then comparitively decreased.

TiO$_2$. Among all the nanocatalysts, NMN-4 showed highest percentage of degradation. The apparent rates were estimated from the slopes of individual curves. Based on the above analysis, a reasonable explanation of the optimal N and Mn content is that, with over dosage of doped content in TiO$_2$, the number of e^-/h^+ recombination centers will increase which results in low photocatalytic activity.

2.5.2. Effect of pH. Figure 5(b) shows the percentage degradation of methyl red as function of time at different pH values. The sample exhibiting best photocatalytic performance (NMN-4) was selected and further experiments were conducted to find out the optimum pH at constant dye concentration (10 mg/L) and catalyst weight (1.0 g/L). It can be seen from the figure that photodegradation of this anionic dye was faster at pH 4. During a photocatalytic oxidation, electrostatic interactions between a semiconductor surface, substrate, and charged radicals strongly depend on the pH of the solution. In acidic environment, positive charge on TiO$_2$ surface increases which enhances the adsorption of

dye molecules on the surface of catalyst. In addition, acidic medium minimizes the e^-/h^+ recombination. The increase of pH renders TiO$_2$ surface negatively charged and the repulsion could occur with dye molecules leading to low adsorption of molecules and thus decrease the degradation efficiency. So, optimization of pH maximizes the photocatalytic performance

2.5.3. Effect of Catalyst Dosage. An optimum catalyst concentration must be determined in order to avoid the catalyst wastage and ensure the total absorption of photons. Photocatalytic degradation experiments carried out with varying amounts (0.25–3.00 g/L) of NMN-4 at pH 4 are represented in Figure 5(c). The rate of degradation increased linearly with increase in amount of catalyst up to 2.00 g/L. The increase in catalyst dosage generally increases the number of photons absorbed by the catalyst, which in turn increases the generation of electrons and holes and thus increases the number of hydroxyl radicals. And also, the increase in catalyst dosage increases the number of organic pollutants adsorbed and facilitates the photocatalytic activity. However, after 2.00 g/L of catalyst dosage, the photocatalytic activity decreased due to the turbidity, restriction of light penetration, and agglomeration of catalyst particles. The high catalyst dosage significantly affects the dispersion.

2.5.4. Effect of Initial Concentration of Dye. To determine the optimum initial dye concentration at a fixed catalyst dosage and pH, experiments were carried out with different dye concentrations of 1, 5, and 10 mg/L and results are represented in Figure 5(d). The optimum initial concentration of dye was found to be 5 mg/L and further increase in dye concentration decreased the rate of degradation. A reasonable explanation is as follows: as the pollutant concentration increases, the corresponding ratio of reactive species ($^\bullet$OH) may not be formed at the fixed catalyst dosage. Limitation of surface active sites for the catalytic reaction may also control the degradation of methyl red.

2.6. Photocatalytic Mineralization of Methyl Red. COD was performed using acidic dichromate method to study the
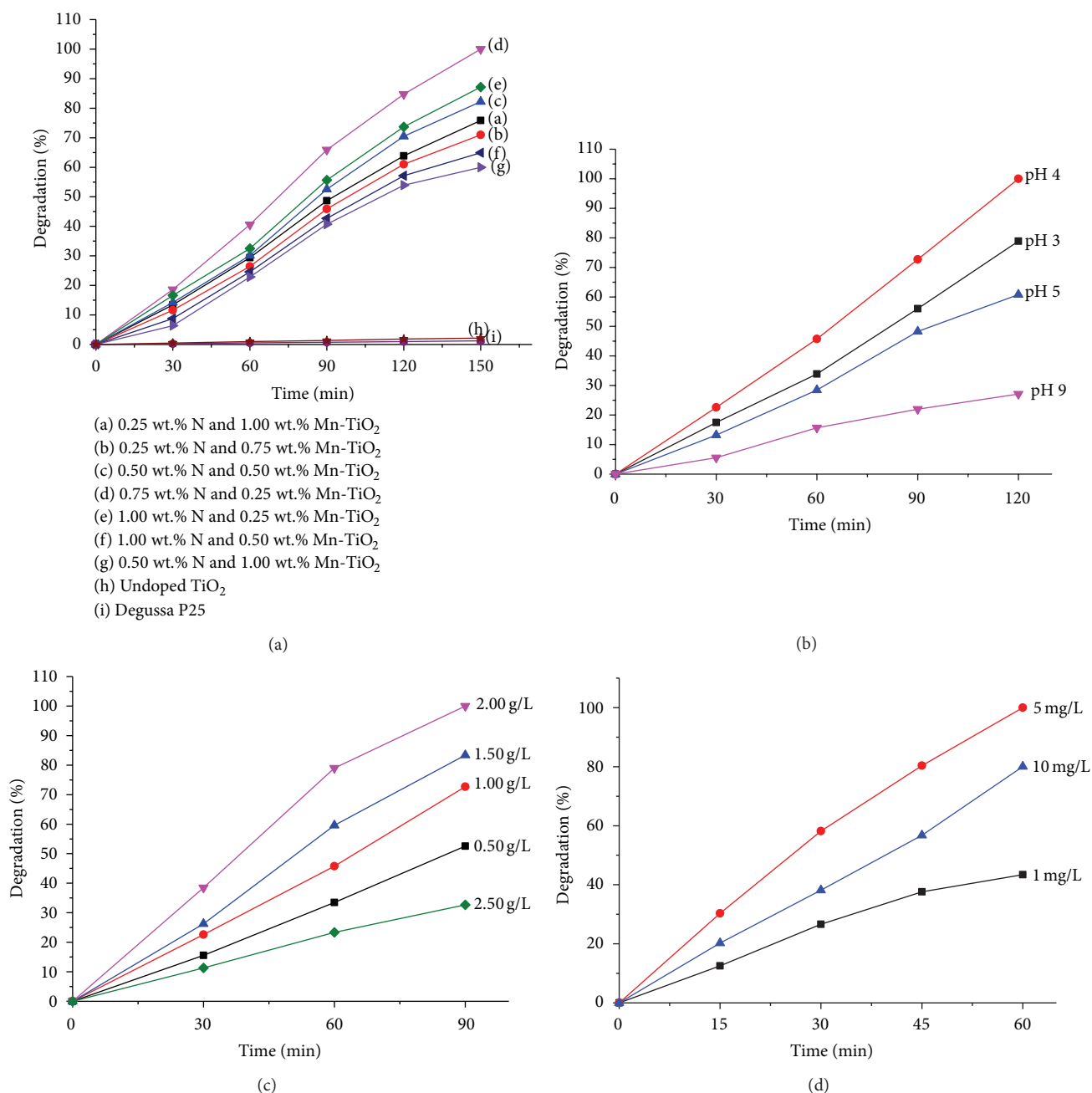
FIGURE 5: The percentage of degradation of methyl red as function of time by N/Mn-TiO$_2$ under different experimental parameters. (a) Effect of Dopant concentration: among all the catalysts with different dopant concentrations, 0.75 wt.% N and 0.25 wt.% Mn-TiO$_2$ (NMN-4) exhibited 100% degradation in 150 min irradiation time. (b) Effect of pH: optimum pH was found to be 4. (c) Effect of catalyst dosage-optimum catalyst dosage was found to be 2.00 g/L. (d) Effect of initial concentration of dye: 5 mg/L of methyl red was degraded completely in 60 min by NMN-4 at pH 4 with catalyst dosage of 0.20 g.

mineralization of methyl red. The mineralization experiments were done by treating methyl red (5 mg/L) with 0.75 wt.% N and 0.25 wt.% Mn-TiO$_2$ (2.00 g/L) at pH 4 under visible light irradiation. The kinetics of total mineralization of methyl red has been followed by the disappearance of COD. The efficiency of degradation was assessed from the experimentally derived COD, measured at regular intervals of visible light exposure. Figure 6 represents the disappearance

of COD with respect to time. It can be seen that there is a gradual reduction in the COD values. However, more time was taken for complete mineralization (90 min) of methyl red when compared with that of degradation (60 min) under same experimental conditions.

2.7. Photocatalytic Degradation of Orange II. In order to once recheck the photocatalytic activity of the synthesized
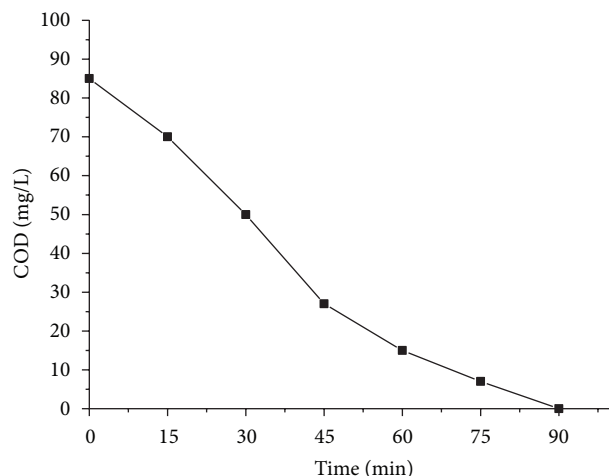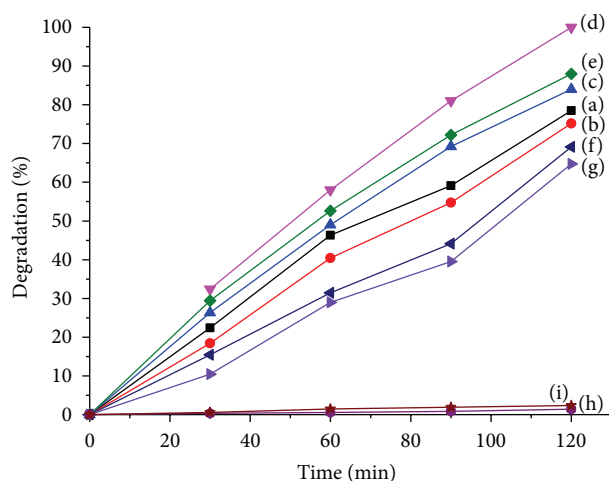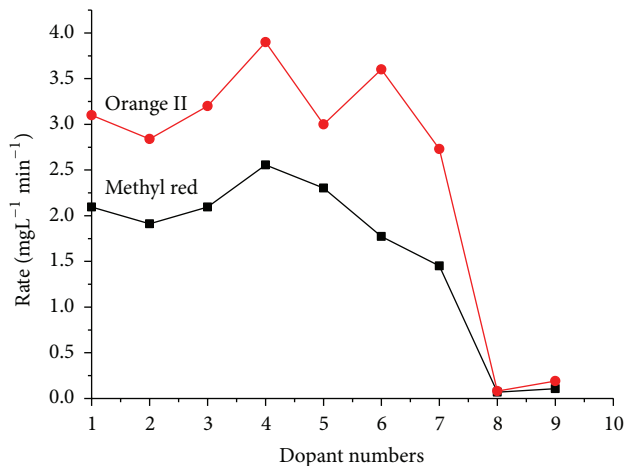
FIGURE 6: Rate of mineralization (COD disappearance) as function of time during degradation of methyl red under visible light. Conditions: [methyl red] = 5 mg/L, N/Mn-TiO$_2$ = 2.00 g/L, pH = 4.

FIGURE 7: Percentage degradation of orange II by photocatalysts with respect to time.

(a) 0.25 wt. % N and 1.00 wt. % Mn-TiO$_2$
(b) 0.25 wt. % N and 0.75 wt. % Mn-TiO$_2$
(c) 0.50 wt. % N and 0.50 wt. % Mn-TiO$_2$
(d) 0.75 wt. % N and 0.25 wt. % Mn-TiO$_2$
(e) 1.00 wt. % N and 0.25 wt. % Mn-TiO$_2$
(f) 1.00 wt. % N and 0.50 wt. % Mn-TiO$_2$
(g) 0.50 wt. % N and 1.00 wt. % Mn-TiO$_2$
(h) Degussa P25
(i) Undoped TiO$_2$

Dopant numbers
(1) 0.25 wt. % N and 1.00 wt. % Mn-TiO$_2$
(2) 0.25 wt. % N and 0.75 wt. % Mn-TiO$_2$
(3) 0.50 wt. % N and 0.50 wt. % Mn-TiO$_2$
(4) 0.75 wt. % N and 0.25 wt. % Mn-TiO$_2$
(5) 1.00 wt. % N and 0.25 wt. % Mn-TiO$_2$
(6) 1.00 wt. % N and 0.50 wt. % Mn-TiO$_2$
(7) 0.50 wt. % N and 1.00 wt. % Mn-TiO$_2$
(8) Degussa P25
(9) Undoped TiO$_2$

FIGURE 8: Comparison of degradation rate of methyl red and orange II by photocatalysts.

when compared with that of methyl red. This is maybe due to the presence of sulphate group in dye orange II which assists in photocatalytic degradation. Thus this experiment also proved that N/Mn-TiO$_2$ can degrade organic dye pollutants.

2.8. Mechanism in Release of $^{\bullet}OH$. Consider

$$\text{Visible light} + \text{Catalyst} \longrightarrow \text{Catalyst} \left(h^+ + e^-\right)$$

$$h^+ + H_2O \longrightarrow H^+ + {}^-OH$$

$$h^+ + {}^-OH \longrightarrow {}^{\bullet}OH$$

$$e^- + O_2 \longrightarrow {}^{\bullet}O_2{}^- \qquad (2)$$

$$e^- + {}^{\bullet}O_2{}^- + H_2O \longrightarrow HO_2{}^{\bullet} + {}^-OH$$

$$e^- + HO_2{}^{\bullet} + H^+ \longrightarrow H_2O_2$$

$$e^- + H_2O_2 \longrightarrow {}^{\bullet}OH + {}^-OH$$

3. Conclusion

Nitrogen and manganese were successfully doped into TiO$_2$ matrix and its photocatalytic activity was studied for the degradation of methyl red under visible light. All the synthesized samples were in anatase phase and band-gap has been reduced. Nitrogen doping caused visible light response and improved the quantum yield. Manganese doping improved

catalysts, a set of experiments were done using another dye, orange II, as target pollutant. The percentage of degradation of dye with respect to time with all the catalysts was represented in Figure 7. In this study also NMN-4 exhibited best photocatalytic activity when compared with the remaining synthesized catalysts. Figure 8 represents the comparative rate of degradation of methyl red and orange II with all the photocatalysts. The rate of degradation is high for orange II
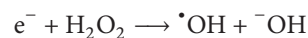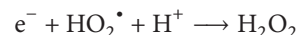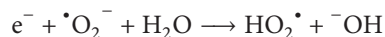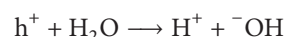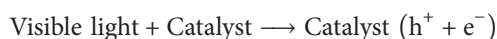
the trapping of electrons inhibiting e^-/h^+ recombination during photocatalytic process. Among all synthesized catalysts 0.75 wt.% N and 0.25 wt.% Mn-TiO$_2$ exhibited excellent photocatalytic activity under visible light due to small particle size, large shift in band gap, high crystalline anatase phase, and effective separation of electrons and holes. 100% degradation of methyl red with initial concentration of 5 mg/L was achieved in 90 min at pH 4 with catalyst dosage of 2.00 g/L. The experimental results revealed that methyl red can be effectively degraded by N/Mn-TiO$_2$ without generation of any hazardous wastes or by-products as evident from the considerable reduction in COD. All the photocatalysts also showed excellent catalytic activity on another dye orange II exhibiting complete degradation. It can be concluded that codoping TiO$_2$ with nitrogen and manganese is a promising route for enhanced photocatalytic degradation of pollutants.

Conflict of Interests

The authors declare that there is no conflict of interests regarding the publication of this paper.

Acknowledgments

References

[1] M. A. Mahmoud, A. Poncheri, Y. Badr, and M. G. Abd El Waned, "Photocatalytic degradation of methyl red dye," *South African Journal of Science*, vol. 105, no. 7-8, pp. 299–303, 2009.

[2] T. Sauer, G. C. Neto, H. J. José, and R. F. P. M. Moreira, "Kinetics of photocatalytic degradation of reactive dyes in a TiO$_2$ slurry reactor," *Journal of Photochemistry and Photobiology A: Chemistry*, vol. 149, no. 1–3, pp. 147–154, 2002.

[3] S. K. Kavitha and P. N. Palanisamy, "Photocatalytic and sonophotocatalytic degradation of reactive red 120 using dye sensitized TiO$_2$ under visible light," *International Journal of Civil and Environmental Engineering*, vol. 3, pp. 1–6, 2011.

[4] C. Kormann, D. W. Bahnemann, and M. R. Hoffmann, "Preparation and characterisation of quantum size titanium dioxide," *The Journal of Physical Chemistry*, vol. 92, no. 18, pp. 5196–5201, 1988.

[5] N. Hariprasad, S. G. Anju, E. P. Yesodharan, and Y. Suguna, "Sunlight induced removal of Rhodamine B from water through semiconductor photocatalysis: effects of adsorption, reaction conditions and additives," *Research Journal of Material Science*, vol. 1, pp. 9–17, 2013.

[6] Y. N. Tan, C. L. Wong, and A. R. Mohamed, "An overview on the photocatalytic activity of nano-doped-TiO$_2$ in the degradation of organic pollutants," *ISRN Materials Science*, vol. 2011, Article ID 261219, 18 pages, 2011.

[7] D. Dvoranova, V. Brezova, M. Mazur, and M. A. Malathi, "Investigations of metal-doped titanium dioxide photocatalysts," *Applied Catalysis B: Environmental*, vol. 37, pp. 91–105, 2002.

[8] J. Zhu, Z. Deng, F. Chen et al., "Hydrothermal doping method for preparation of Cr^{3+}-TiO$_2$ photocatalysts with concentration gradient distribution of Cr^{3+}," *Applied Catalysis B: Environmental*, vol. 62, no. 3-4, pp. 329–335, 2006.

[9] G. Wu, T. Nishikawa, B. Ohtani, and A. Chen, "Synthesis and characterization of carbon-doped TiO$_2$ nanostructures with enhanced visible light response," *Chemistry of Materials*, vol. 19, no. 18, pp. 4530–4537, 2007.

[10] K. R. Patil, S. D. Sathaye, Y. B. Khollam, S. B. Deshpande, N. R. Pawaskar, and A. B. Mandale, "Preparation of TiO$_2$ thin films by modified spin-coating method using an aqueous precursor," *Materials Letters*, vol. 57, no. 12, pp. 1775–1780, 2003.

[11] U. G. Akpan and B. H. Hameed, "The advancements in sol-gel method of doped-TiO$_2$ photocatalysts," *Applied Catalysis A: General*, vol. 375, no. 1, pp. 1–11, 2010.

[12] H. Natori, K. Kobayashi, and M. Takahashi, "Preparation and photocatalytic property of phosphorus-doped TiO$_2$ particles," *Journal of Oleo Science*, vol. 58, no. 7, pp. 389–394, 2009.

[13] K. R. Reyes-Gil, E. A. Reyes-García, and D. Raftery, "Photoelectrochemical analysis of anion-doped TiO$_2$ colloidal and powder thin-film electrodes," *Journal of the Electrochemical Society*, vol. 153, no. 7, pp. A1296–A1301, 2006.

[14] Q. R. Deng, X. H. Xia, M. L. Guo, Y. Gao, and G. Shao, "Mn-doped TiO$_2$ nanopowders with remarkable visible light photocatalytic activity," *Materials Letters*, vol. 65, no. 13, pp. 2051–2054, 2011.

[15] J. Wang, D. N. Tafen, J. P. Lewis et al., "Origin of photocatalytic activity of Nitrogen-doped TiO$_2$ nanobelts," *Journal of the American Chemical Society*, vol. 131, no. 34, pp. 12290–12297, 2009.

[16] J. F. Moulder, W. F. Stickle, P. E. Sobol, and K. D. Bomben, *Handbook of X-Ray Electron Spectroscopy*, PerkinElmer, Eden Prairie, Minn, USA, 1992.

[17] H. Czili and A. Horváth, "Applicability of coumarin for detecting and measuring hydroxyl radicals generated by photoexcitation of TiO$_2$ nanoparticles," *Applied Catalysis B: Environmental*, vol. 81, no. 3-4, pp. 295–302, 2008.

International Journal of
Medicinal Chemistry

Organic Chemistry
International

International Journal of
Photoenergy

International Journal of
Analytical Chemistry

Advances in
Physical Chemistry

International Journal of
Carbohydrate
Chemistry

Journal of
Quantum Chemistry

The Scientific
World Journal

Journal of
Analytical Methods
in Chemistry

Submit your manuscripts at
http://www.hindawi.com

Hindawi

Journal of
Spectroscopy

International Journal of
Inorganic Chemistry

International Journal of
Electrochemistry

Journal of
Applied Chemistry

Bioinorganic Chemistry
and Applications

Journal of
Theoretical Chemistry

Chromatography
Research International

Journal of
Catalysts

Journal of
Chemistry

International Journal of
Spectroscopy